Probabilistic fatigue assessment of rib-to-deck joints using thickened edge U-ribs

Heng, Junlin; Zheng, Kaifeng; Kaewunruen, Sakdirat; Zhu, Jin; Baniotopoulos, Charalampos

DOI:
10.12989/scs.2020.35.6.799

Document Version
Peer reviewed version

Citation for published version (Harvard):
Heng, J, Zheng, K, Kaewunruen, S, Zhu, J & Baniotopoulos, C 2020, 'Probabilistic fatigue assessment of rib-to-deck joints using thickened edge U-ribs', *Steel & Composite Structures: an international journal*, vol. 35, no. 6, pp. 799-813. https://doi.org/10.12989/scs.2020.35.6.799

Probabilistic fatigue assessment of rib-to-deck joints using thickened edge U-ribs

Junlin Heng[1,2a], Kaifeng Zheng[*1], Sakdirat Kaewunruen[2], Jin Zhu[1], and Charalampos Baniotopoulos[2]

[1]*Department of Bridge Engineering, School of Civil Engineering, Sou thwest Jiaotong University, Chengdu, China*

[2]*Department of Civil Engineering, School of Engineering, University of Birmingham, Birmingham, UK*

(Received keep as blank , Revised keep as blank , Accepted keep as blank)

Abstract. Fatigue cracks of rib-to-deck (RD) joints have been frequently observed in the orthotropic steel decks (OSD) using conventional U-ribs (CU). Thickened edge U-rib (TEU) is proposed to enhance the fatigue strength of RD joints, and its effectiveness has been proved through fatigue tests. In-depth full-scale tests are further carried out to investigate both the fatigue strength and fractography of RD joints. Based on the test result, the mean fatigue strength of TEU specimens is 21% and 17% higher than that of CU specimens in terms of nominal and hot spot stress, respectively. Meanwhile, the development of fatigue cracks has been measured using the strain gauges installed along the welded joint. It is found that such the crack remains almost in semi-elliptical shape during the initiation and propagation. For the further application of TEUs, the design curve under the specific survival rate is required for the RD joints using TEUs. Since the fatigue strength of welded joints is highly scattered, the design curves derived by using the limited test data only are not reliable enough to be used as the reference. On this ground, an experiment-numerical hybrid approach is employed. Basing on the fatigue test, a probabilistic assessment model has been established to predict the fatigue strength of RD joints. In the model, the randomness in material properties, initial flaws and local geometries has been taken into consideration. The multiple-site initiation and coalescence of fatigue cracks are also considered to improve the accuracy. Validation of the model has been rigorously conducted using the test data. By extending the validated model, large-scale databases of fatigue life could be generated in a short period. Through the regression analysis on the generated database, design curves of the RD joint have been derived under the 95% survival rate. As the result, FAT 85 and FAT 110 curves with the power index *m* of 2.89 are recommended in the fatigue evaluation on the RD joint using TEUs in terms of nominal stress and hot spot stress respectively. Meanwhile, FAT 70 and FAT 90 curves with *m* of 2.92 are suggested in the evaluation on the RD joint using CUs in terms of nominal stress and hot spot stress, respectively.

Keywords: orthotropic steel deck; rib-to-deck joint; thickened edge U-rib; probabilistic fatigue assessment;

1. Introduction

Orthotropic steel decks (OSDs) have been extensively applied in steel bridges worldwide, due to their excellent performance such as light self-weight, speedy construction, high redundancy,

*Corresponding author, Professor, E-mail: kfzheng@home.swjtu.edu.cn

[a] Ph.D. Student, E-mail: j.l.heng@foxmail.com

good capacity and so on (Connor *et al.* 2012). After the second world war, the OSD gradually become a crucial symbol of modern steel bridges. However, the application of OSDs is not always problem-free. Due to their complicated details and the massive welding works involved, fatigue cracking is frequently observed in the welded joint in OSDs. Among various types of cracks, special attention has been paid to the fatigue crack in rib-to-deck (RD) joints. The crack in RD joints is probably induced by the following two reasons. Firstly, the RD joint accounts for the largest proportion of welded joints in OSDs, which are more prone to fatigue than other types of joints under the cyclic traffic loads. Secondly, because of the direct contact with the wheel load, the local effects are quite significant, which increase the possibility of fatigue cracking in the RD joint. Subsequently, those fatigue cracks in the RD joint could result in serious consequences, e.g., the degradation of serviceability and even failure of the whole deck system.

In recent years, several works have been carried out to improve the fatigue performance of RD joints. These works mainly fall into two categories, i.e., the manipulation of different penetration rate and the implementation of ultrahigh-performance concrete (UHPC) layer. Cao *et al.* (2015) proposed a new welding technology to achieve full penetration with the controlled weld-melt-through. Based on the fatigue tests of four specimens, the authors claimed that the fatigue life of the specimens using the proposed full penetration increased by 200%. Kainuma *et al.* (2016) investigated the effect of the full penetration on the fatigue performance of RD joints. Full-scale fatigue tests were carried out, and the result suggested that full penetration has a negative influence on the fatigue performance of RD joints. Luo *et al.* (2018) studied the fatigue performance of the two-sides welding by using numerical analysis. The authors proposed that since the maximum effective notch stress was decreased by 19% when using the two-sides welding, the fatigue performance of rib-to-deck joints could be enhanced. However, both the penetration rate or the number of welding sides seem to have little influence on the fatigue strength of RD joints. As proposed by Tang (2011), the limited thickness of the U-rib may be the cause. Since the 8 mm-thick U-rib is generally used in OSDs, the penetration depth of the rib wall only increased by 2 mm even after employing full penetration or two-sides welding.

Meanwhile, the OSD with ultrahigh-performance concrete (UHPC) was proposed (Shao *et al.* 2015). UHPC is a kind of innovative concrete with advanced mechanical properties (Meng *et al.* 2016). In the system, the UHPC layer and deck plate are composited by shear studs, so that they could work together against the applied vehicle loading (Xiaochen and Zhibing 2014; Qinghua *et al.* 2016). According to the test result, the vehicle-induced cyclic stress in rib-to-deck joints was remarkably decreased (Zhang *et al.* 2017). However, one of the major concerns is that the self-weight of the deck system increases significantly due to the employment of the UHPC layer, and consequently restricts its further application on the long-span bridges. Moreover, cracking of the UHPC layer and failure of the shear studs would happen under the cyclic loading (Chen *et al.* 2017; Bing *et al.* 2017). As the result, the cyclic stress in rib-to-deck joints may gradually increase and finally reach the level as in the joints without the UHPC layer (Zhang *et al.* 2017).

To solve the problem, a new type of thickened edge U-rib (TEU) has been designed and manufactured (Wang *et al.* 2015; Heng *et al.* 2017), as shown in Figs. 1(a)-(c). Generally, the conventional U-rib (CU) with an 8 mm-thick wall is used in OSDs. In comparison with the CU, the wall thickness near the joint is increased by 50% (from 8 to 12 mm) in the TEU. As the result, a larger welding depth could be achieved under the same un-fused length. Such treatment aims to reduce the stress level and improve the fatigue performance of the joints, without significantly increasing the self-weight of the deck system. The thickened edge of TEUs is formed by the continuously rolling method using a group of rollers, as illustrated in Fig. 1c. Manufacturing cost

is not obviously increased since only the edge of plates is under special treatments. In addition, a smooth transition is generated near the joint, which is beneficial for the fatigue performance.

(a) Sectional view (b) Photography (c) Fabrication process

Fig. 1 Illustration of TEUs

However, an in-depth evaluation of the fatigue performance of the rib-to-deck joint using TEUs is still required due to the lack of study in this field. Usually, the fatigue test is believed as a crucial and trustable approach in the fatigue evaluation (Connor *et al.* 2012). The major issue is that it is both time and budget consuming to conduct a comprehensive fatigue test. Meanwhile, due to the stochastic nature of fatigue performance, a large size of test data is required to obtain a desirable design stress-life curve. As an alternative, the numerical method is frequently employed. Recently, fracture mechanics has been intensively used in combination with the probabilistic analysis. Righiniotis and Chryssanthopoulos (2003) suggested that the fracture mechanics-based probabilistic analysis could be employed to predict the fatigue life of welded details. Liu and Mahadevan (2009) proposed a probabilistic crack growth model based on fracture mechanics. In the model, the final crack was assumed to be developed from a single initial flaw, which could be called “single-crack assumption”. The model was applied to calculate the fatigue life of smooth plate specimens, and the result was validated by experimental data. Maljaars and Voruwenvelder (2014) proposed a probabilistic fracture model basing on the single-crack assumption, to predict the fatigue life of rib-to-floor beam welded joints in OSDs. Sanches *et al.* (2015) conducted fatigue life prediction of riveted joints using a proposed probabilistic fracture model, in which the single-crack assumption was also employed. Baptista *et al.* (2017) employed a probabilistic fracture model under the single-crack assumption, to induce the S-N curves of flange tip attachments in steel truss bridges.

As stated above, fatigue evaluation is required on the actual performance of the rib-to-deck (RD) joint using TEUs. Moreover, the design stress-life (S-N) curves under survival rates are needed for the fatigue design of this type of joint. The objective of this study is to evaluate fatigue performance of the RD joint using TEUs, and to generate the design S-N curves as the guideline for fatigue design. In the study, an experiment-numerical hybrid approach has been employed to improve the accuracy and efficiency. Comparative fatigue tests have been firstly performed for both the CU and TEU specimens, which validates the effectiveness of TEUs in enhancing the fatigue performance of rib-to-deck joints. Furthermore, in-depth full-scale fatigue tests have been carried out to investigate both the fatigue strength and fractography of RD joints. Subsequently, the experimental data have been used to develop a data-driven probabilistic assessment model basing on the fracture mechanics. In the model, the multiple-sites initiation and coalescence of fatigue cracks are considered to improve the accuracy. The validity of the proposed model has been rigorously checked using the test data. With the verified model, large-scale databases of fatigue life could be generated in a short period of time. Through regression analysis on the

generated database, the design curves of RD joints have been generated under the specific survival rate, which could be used as references in the fatigue design.

2. Fatigue tests on rib-to-deck specimens

2.1 Preliminary fatigue studies

Fatigue tests of full-scale rib-to-deck specimens have been carried out to evaluate the effect of TEUs on the fatigue performance of rib-to-deck joints (Heng et al. 2017). Three specimens using CUs and four specimens using TEUs are manufactured using the structural steel Q345qD (GB/T 714 2015). The TEU and CU specimens are designated as TEU-1 to TEU-4 and CU-1 to CU-3, respectively. Constant amplitude cyclic loads have been applied under a stress ratio of 0.3. In all the specimens tested, fatigue cracks firstly initiate at the deck toe, and then propagate in both the longitudinal and vertical direction of deck plates until the crack penetrates through the thickness. The failure is assumed when the first penetrating crack can be detected. Through the multiple strain gauges placed in front of the deck toe, fatigue strength is measured in terms of nominal stress and hot spot stress (Bing *et al.* 2015) respectively. As shown in Fig. 2, the test data are plotted against three FAT curves (CEN 2005), where the abbreviations "NS" and "HS" respectively stand for nominal stress and hot spot stress. In terms of nominal stress, all the four data points of the TEU specimens are well above the curve FAT 100, while only one data point of the CU specimens is above the curve. After replacing the curve FAT 100 by the curve FAT 125, the same trend could be observed in terms of hot spot stress. Therefore, the experimental results indicate that the fatigue performance of the rib-to-deck is improved after using the TEU.

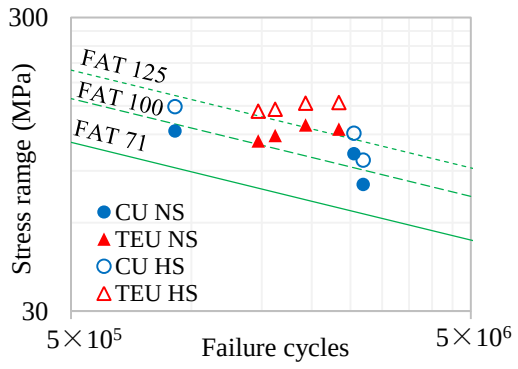

Fig. 2 Stress-life data obtained from the preliminary test

2.2 In-depth full-scale experiments

The preliminary tests have qualitatively indicated that the employment of TEUs could effectively improve the fatigue performance of rib-to-deck joints. To further evaluate the performance of TEUs in a quantitative way, in-depth full-scale tests are carried out to investigate the fatigue strength and the typical cracking pattern of rib-to-deck joints. Four full-scale rib-to-

deck specimens, two using TEUs and two using CUs, have been fabricated with the structural steel Q345qD (GB/T 714 2015). In accordance with the preliminary tests, the specimens are designated as CU-4, CU-5, TEU-5 and TEU-6. The welding parameters and procedures are kept the same as those used in the fabrication of the previous specimens.

The specimen is fixed to the testing plate using the Grade 10.9 high-strength bolts (JGJ 82 2011), which are 16 mm in diameter, as shown in Fig. 3. The actuator is placed at the centre of the left joint, with a rubbery plate installed underneath to distribute the applied load. Similarly, constant amplitude loads are employed during the tests, as shown in Table 1.

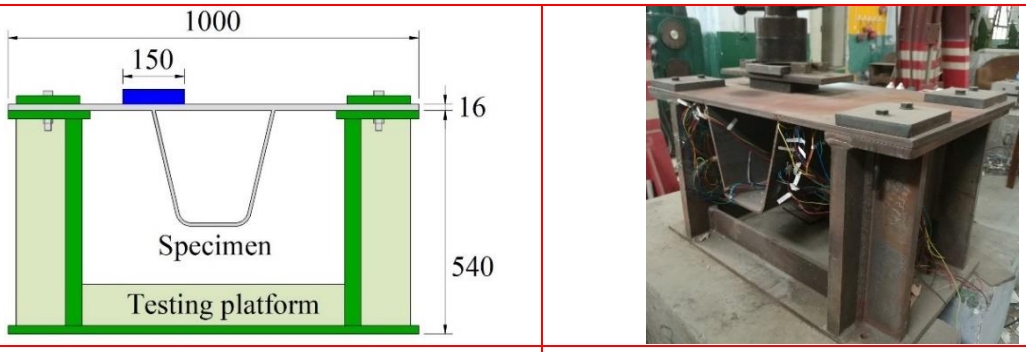

(a) Sectional view (unit: mm) (b) Photograph

Fig. 3 Set-up of the in-depth test

Table 1 Applied loads (kN)

Code	F_{min}*	F_{max}	F_{max} - F_{min}
CU-4	15	50	35
CU-5	20	65	45
TEU-5	20	60	40
TEU-6	30	85	55

*F_{min}: Minimum load; F_{max}: Maximum load.

Resistive electric strain gauges are used, as shown in Figs. 4(a)-(b). The strain data are collected using the dynamic data logger DH5921 during the test. Three sections, i.e., north section, middle section and south section, are identified as the critical sections of the specimen. The gauges at each selected section are arranged in the same way as shown in Fig. 4(a). According to the previous tests, the fatigue crack is expected to initiate at the deck toe and then propagate in both the length and depth of the deck plate. Therefore, a series of gauges spacing 7.5 mm along the joint are installed in front of the deck toe. Through these gauges, the changes in strain have been monitored during loading, which could in turns reflect the development of fatigue cracks (Cao *et al.* 2015). The gauges placed in front of the deck toe are designed as D24 and D8-X, where the letter 'X' stands for the numbers counting from 1 to 79.

Since two gauges are placed in front of the deck toe, both nominal stress and hot spot stress could be measured and calculated (Niemi *et al.* 2006). The nominal stress is determined using the gauges D24, which is placed at the distance of 1.5 times the plate thickness (24 mm) away from the deck toe. Meanwhile, the linear extrapolation suggested by Hobbacher (2015) is used to

calculate the hot spot stress, as shown in Eq. 1.

$$\sigma_{hs} = 1.5\sigma_{0.5t} - 0.5\sigma_{1.5t} \#(1)$$

where t stands for the thickness of deck plates (16 mm); σ_{hs} is the hot spot stress; $\sigma_{0.5t}$ and $\sigma_{1.5t}$ are the stress measured at the distance of 0.5 and 1.5 times the plate thickness away from the deck toe respectively, i.e., D8-X and D24 in this study.

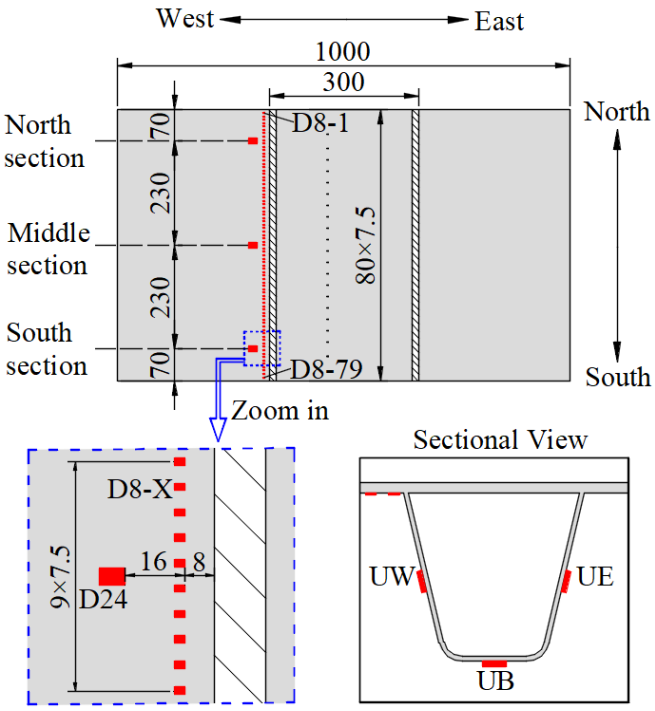

(a) Illustration (unit: mm)

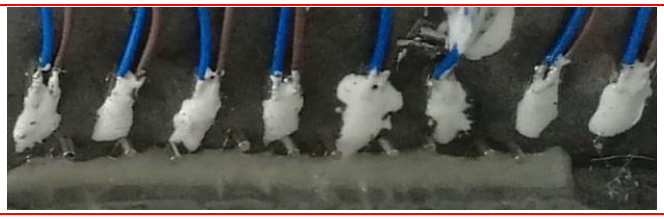

(b) Photography

Fig. 4 Arrangement of strain gauges

During the tests, dye penetration checks are firstly performed every 50 thousand cycles to identify the fatigue crack and then carried out every 10 thousand cycles after the first crack is detected. The failure criterion is the same as the previous one: the specimens are assumed to be failed once the first penetrated crack is identified. As shown in Fig. 5, the cracking pattern is the same as the previous tests: cracks firstly initiate at the deck toe and then propagate in the length and depth of deck plates until penetrating through the entire thickness.

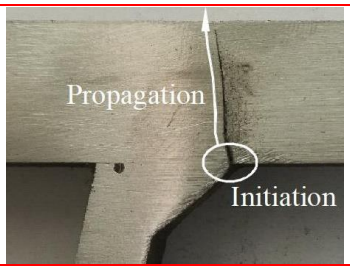

Fig. 5 Cracking pattern measured on the macro-section of CU-4

2.3 Test results

In the test, as the fatigue crack initiates and propagates, the strain near the cracking location will be gradually released, which could lead to strain drops in the nearby gauges. During the cyclic loading, the strain drops along the deck toe have been measured and then used to reflect the crack development. Statistic tests is conducted before the cyclic loading, and the strain data measured in the statistic test are used to calculate the ratio of strain drops, as shown in Eq. 2.

$$\delta_{dr} = (1 - \varepsilon_{test}/\varepsilon_{stat}) \times 100\% \#(2)$$

where δ_{dr} stands for the ratio of strain drops; ε_{test} and ε_{stat} are the strain range measured during the cyclic loading and in the static loading respectively.

The strain drops measured during the tests are summarized in Figs. 6(a)-(d). Since it is unable to install the gauges at the two ends of specimens due to the narrow space, the value at the ends (distance = ±300 mm) is represented by the ratio of cracked thickness to the whole thickness, which is measured using dye penetration checks. The result shows that the fatigue crack firstly occurs near one of the two ends randomly, and then propagates in both vertical and longitudinal directions of the deck plate. After the detection of the first crack, the second crack will be identified at another end, and then the two cracks propagate simultaneously. Obviously, the first crack propagates faster than the second one, and the failure is reached when the first crack penetrates through the thickness of the deck plate. Meanwhile, it is worth noting that in all the specimens, the crack almost remains in the semi-elliptical shape during the development.

The fatigue strength of the joint is defined by the stress range measured at the section where the first penetrated crack is observed. The results are summarized in Table 2, including the data obtained from the previous test. According to Eurocode 3 (CEN 2005), stress-life curves can be named after the fatigue strength at 2 million cycles (FAT). Based on this concept, the equivalent fatigue strength of the specimens is calculated using Miner's law (Hobbacher 2015), as shown in Eq. 3.

$$\Delta\sigma_{eqv} = \left(\frac{N_{test}}{N_{eqv}}\right)^{\frac{1}{m}} \cdot \Delta\sigma_{test} \#(3)$$

where $\Delta\sigma_{eqv}$ stands for the equivalent fatigue strength; $\Delta\sigma_{test}$ and N_{test} stand for the measured stress range and failure cycle, respectively; N_{eqv} is the equivalent failure cycle, taken as 2×10^6 in this study; m is the material constant, assumed to be 3.0 as a common practice.

Based on the result, in terms of nominal and hot spot stress, the mean equivalent fatigue strength of TEU specimens is respectively 21% and 17% higher than that of CU specimens.

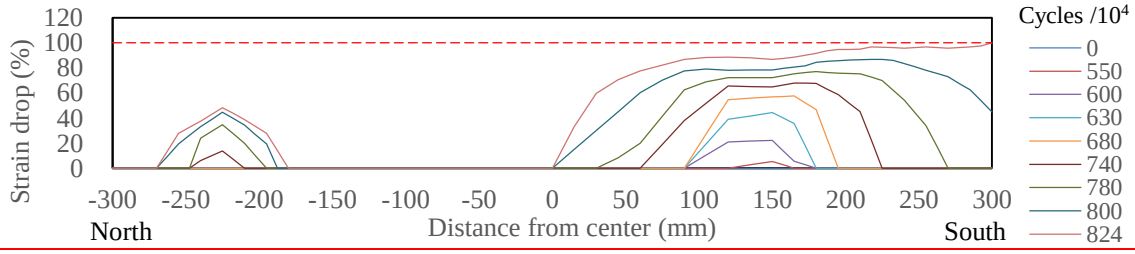

(a) CU-4

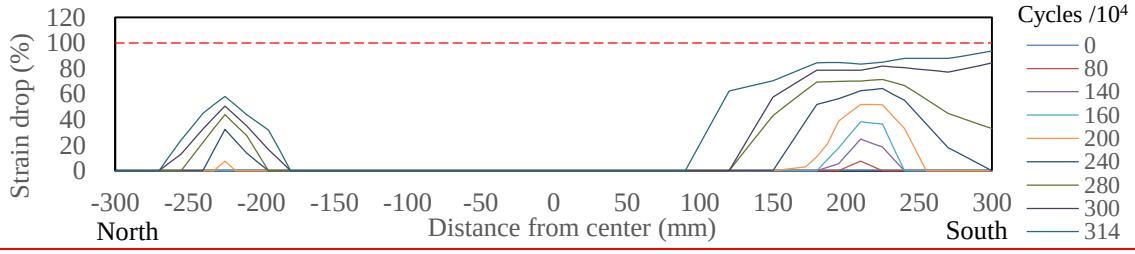

(b) CU-5

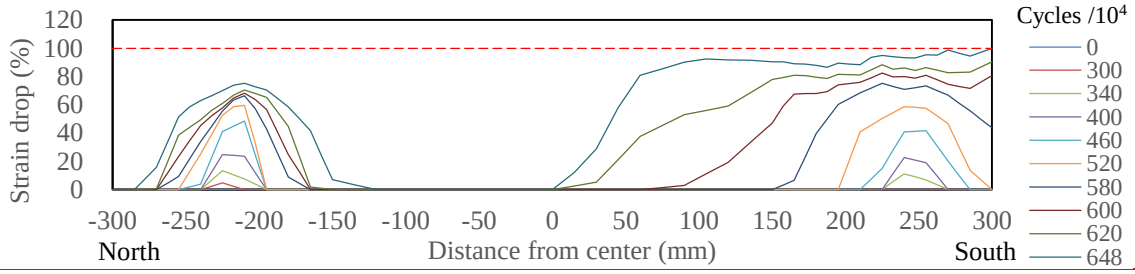

(c) TEU-5

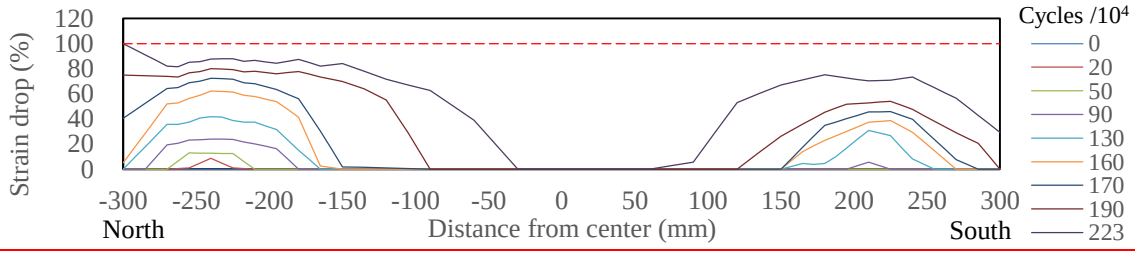

(d) TEU-6

Fig. 6 Strain drops measured in the specimens

Obviously, it is unsafe to use the mean fatigue strength directly in the design, since the mean only represents the 50% survival rate. Alternative, the design value should be generated under the specific survival probability to consider the safety margin sufficiently. Thus, the mean curve and the design curve are generated by performing regression analysis on the test data (Hobbacher 2015). In the regression, the log-linear model is assumed for stress-life relations, as shown in Eq. 4.

$$log\, N = log\, C - m \cdot log\, \Delta\sigma \quad \#(4)$$

where N stands for the fatigue life; C and m are the material constant and power index respectively; $\Delta\sigma$ is the applied stress range.

Table 2 Test results

CODE	Measured stress range		Failure cycles	Equivalent fatigue strength		Mean equivalent fatigue strength	
	$\Delta\sigma_{ns}$ (MPa)	$\Delta\sigma_{hs}$ (MPa)	N_{test} ($\times 10^4$)	$\Delta\sigma'_{ns}$ (MPa)	$\Delta\sigma'_{hs}$ (MPa)	$\Delta\sigma_{ns}$ (MPa)	$\Delta\sigma_{hs}$ (MPa)
CU-1	81	98	269	89	108	96 (8.8*)	123 (10.9)
CU-2	103	121	255	112	131		
CU-3	123	149	91	95	115		
CU-4	58	81	824	92	129		
CU-5	81	113	314	94	132		
TEU-1	114	144	147	103	130	116 (11.1)	144 (12.2)
TEU-2	119	146	162	111	136		
TEU-3	125	154	234	132	162		
TEU-4	129	153	193	127	151		
TEU-5	78	101	650	116	149		
TEU-6	106	131	223	110	135		

*the values in brackets are standard deviations

Since the data points are limited, the power index m is assumed to be 3.0, according to Hobbacher (2015). Under this assumption, the mean value and standard derivation of $log\,C$ can be calculated. Consequently, the design value of $log\,C$ has been derived using Eq. 5.

$$x_d(log\,C) = x_m(log\,C) - k \cdot Std(log\,C) \#(5)$$

where x_d and x_m are the design value and mean value, respectively; Std is the standard deviation; k is the characteristic factor derived by the statistical theory.

In several codes, the characteristic factor $k = 2$ is used, which is the critical value of the normal distribution at 97.7% survival rate. Since the sample mean and sample variance are used instead of the real values, the randomness in the estimators is ignored in this method. In order to improve the accuracy, the randomness in both the data and estimators are considered (Hobbacher 2015). The characteristic factor k is calculated under a survival rate of 95%, and the distribution of the estimators is considered using the two-sided 75% tolerance limit, as shown in Eq. 6.

$$k = t_{p,n-1}/\sqrt{n} + \Phi_{\alpha}^{-1} \cdot \sqrt{(n-1)/\chi^2_{(1+\beta)/2,n-1}} \#(6)$$

where $t_{p,n-1}$ is the critical value of *t*-distribution with $n-1$ degrees at the confidence level p; Φ_{α}^{-1} is the critical value of normal distribution at the confidence level α; $\chi^2_{(1+\beta)/2,n-1}$ is the critical value of chi-square distribution with $n-1$ degrees at the confidence level $(1+\beta)/2$; n is the size of sample; $\alpha = 0.95$ and $p = \beta = 0.75$ are used in this study.

The test data are plotted against the regression curves in Figs. 7(a)-(b). In terms of both nominal and hot spot stress, the mean curve and the design curve of TEU specimens are well above those of CU specimens, indicating the higher fatigue strength of TEU specimens. Meanwhile, the FAT value has been calculated using the generated curves. In the case of mean curves, the FAT values of TEU specimens are 21% and 17% higher than that of CU specimens in terms of nominal and hot spot stress, respectively. In the case of design curves, the FAT values of TEU specimens are 19% higher than that of CU specimens in terms of both nominal and hot spot stress. According to the comparisons in the mean equivalent fatigue strength and the regression

curves, the fatigue strength of rib-to-deck joints can be effectively enhanced by using TEUs.

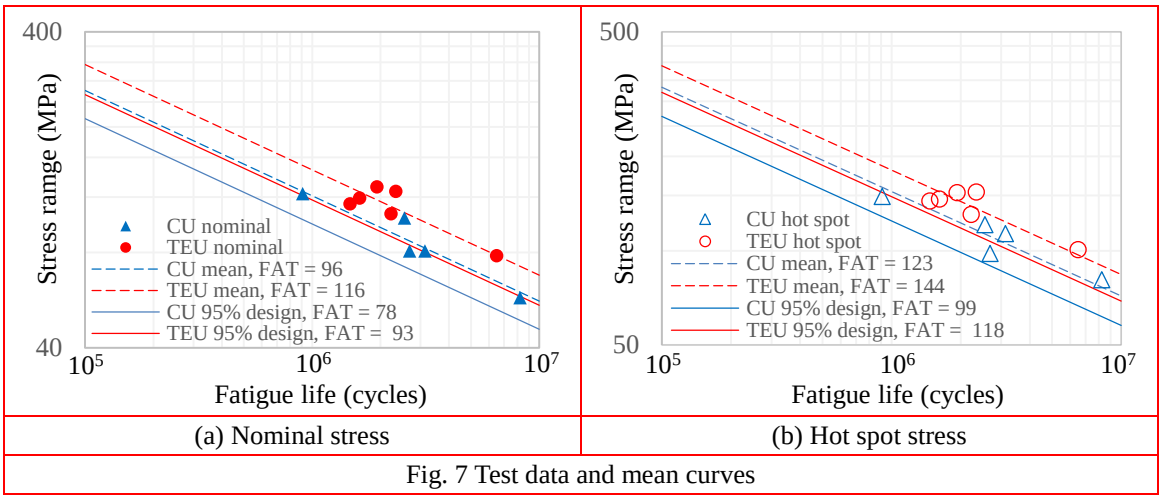

(a) Nominal stress (b) Hot spot stress

Fig. 7 Test data and mean curves

However, due to the highly stochastic nature of fatigue strength, the design curves derived using the limited test data only are not reliable enough to be used as the reference. As an alternative solution, an experiment-numerical hybrid approach is employed in this study. Based on the test data, a probabilistic assessment model has been established to generate the design stress-life curves of rib-to-deck joints, which is introduced in detail in the following sections.

3. Probabilistic fatigue assessment model

3.1 Fatigue crack growth model

Since fatigue cracks can be observed at deck toes in the tests, they are assumed to be developed from the initial flaws existed at the deck toe, as shown in Fig. 8. Considering the measured crack shape, the semi-elliptic propagation model, with two degrees of freedom in the crack tip and edge, is applied in the study. In fracture mechanics, stress intensity factors (SIFs) are regarded as the driving force of crack propagation (Anderson 2005). Generally, the SIFs could be solved directly by the finite element (FE) analysis using the cracked model, in which the crack body is modelled (ANSYS 2018a). Since the SIFs change with the crack geometries during the propagation, the fatigue evaluation should be performed step-by-step (Nagy *et al.* 2015). In the analysis, limitations should be imposed on the maximum increment of each step to achieve the desired accuracy. In the deterministic assessment, the computational cost of the FE method is high but somehow acceptable when the high-performance computer is available. As it comes to the probabilistic fatigue assessment, since large-scale simulations are required to account for the high randomness, the computational cost becomes too high that restricts the application of the direct FE method. Alternatively, derived solutions of SIFs could be used in combination with the stress results obtained from the uncracked FE model (Baik 2011; Hobbacher 2015; BS 7910 2015). In this study, the SIFs are calculated using the method proposed in BS 7910 (2015), as shown in Eq. 4. The solutions proposed by Bowness and Lee (2000) are used to calculate the weld toe magnification factors, and the other parameters in Eq. 7 can be found in BS 7910 (2015).

$$K_i = Mf_w\left(M_{m,i}M_{km,i}\sigma_m + M_{b,i}M_{kb,i}\sigma_b\right)\sqrt{\pi a}\#(7)$$

where the subscript i = a or c, standing for the crack tip or crack edge; K stands for the stress intensity factor; M is the bulging correction factor; f_w is the finite width correction factor; $M_{m,i}$ and $M_{b,i}$ are the correction factors for the crack shape considering the membrane and bending stress respectively; $M_{km,i}$ and $M_{kb,i}$ are the weld toe magnification factors for the membrane and bending stress respectively; σ_m and σ_b stand for the membrane and bending stress, respectively; a stands for the cracking depth.

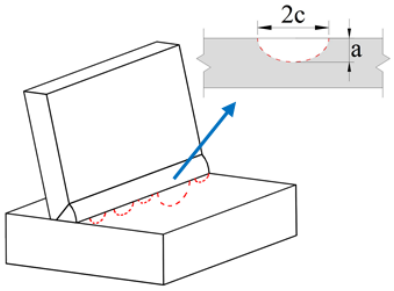

Fig. 8 Fatigue crack model

According to the studies (Pang *et al.* 2017; Madia *et al.* 2018), the development of fatigue cracks could be divided into two stages when considering the dimension of cracks. At the first stage, small cracks initiate from the initial flaws existed at multiple sites. Those small cracks are unable to be detected using normal means. At the second stage, the small cracks gradually merge into main cracks, and the main cracks then propagate in the depth and width until failure. Most of the current studies focus only on the second stage, which leads to the assumption of "single-crack". Under the assumption, the cracking site should be artificially defined in advance, which is contradicted to the stochastic nature of fatigue cracking. Dealing with the problem, in this study, the fatigue cracks are assumed to initiate from the initial flaws located at multiple sites along the joint, as shown in Fig. 8.

In simulating the coalescence of cracks during propagation, the criterion of "equal area" has been employed (Kamaya 2008). Fig. 9 illustrates the criterion in details, where the letter 'S' stands for the area of semi-elliptical cracks; the letters 'a' and 'c' stand for the crack depth and width respectively. Once the overlap of any two cracks are detected, they will be replaced by a new crack, whose area and width are equal to the sums of those in the previous two cracks. Through repeating the process for each crack, the coalescence of cracks could be simulated.

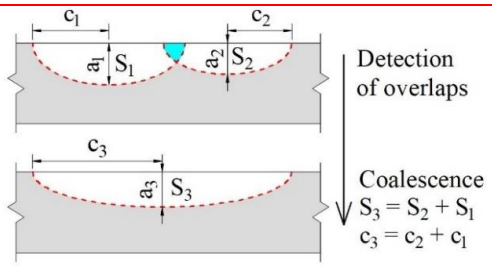

Fig. 9 Illustration of coalescence criterion

In the calculation of propagation rate, the two-stage Paris law suggested in BS 7910 (2015) is employed. The calculation of growth rate at the crack tip is illustrated in Eq. 8, while the same rule is also applied to calculate the growth rate at the crack edge.

$$\frac{da}{dN} = \begin{cases} 0 & \forall \Delta K_a < \Delta K_{th} \\ A_1\left(\Delta K_a^{m_1} - \Delta K_{th}^{m_1}\right) & \forall \Delta K_{th} < \Delta K_a \leq \Delta K_{tr} \\ A_2\left(\Delta K_a^{m_2} - \Delta K_{th}^{m_2}\right) & \forall\, \Delta K_{tr} < \Delta K_a \end{cases} \#(8)$$

where A and m are material constants and power factor respectively, and their subscript 1 and 2 stand for the propagation stage 1 and 2 respectively; ΔK_a is the stress intensity factor at the crack tip; ΔK_{th} stands for the fatigue threshold, below which the crack will not grow; ΔK_{tr} stands for the transition threshold between stage 1 and stage 2.

The transition threshold is a dependent variable, which could be determined by the value of material constants in two stages, as shown in Eq. 9.

$$\Delta K_{tr} = \sqrt[m1-m2]{A_2/A_1} \#(9)$$

3.2 Probabilistic model

In the probabilistic model, parameters describing the local weld geometries, initial flaws and material properties are taken as random variables. In the study, local geometries are represented by the idealized configuration illustrated in Fig 10.

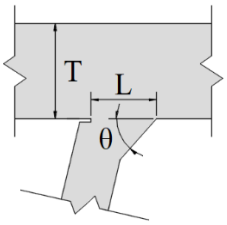

Fig. 10 Idealized configuration of rib-to-deck joints

After tested, the specimens have been cut into pieces, and the local geometries are measured on the macro-sections, as shown in Fig. 5. The measured local geometries are listed in Table 3. For the unbiasedness in estimators, the average value and the sample variance are used as the estimator of the mean and variance. The assumption of the normal distribution is applied to the local geometries as a common practice (Devore 2011).

In case of the material properties, the distributions of growth rate *A* and power index *m* is deduced from the mean and design value suggested in BS 7910 (2015), in which the index *m* is fixed and the growth rate *A* accounts for all the randomness in the crack propagation. According to the studies (Austen 1983; Walbridge 2005; Maljaars *et al.* 2014), the lognormal distribution is applied to the fatigue threshold K_{th}. For welded joints, the influence of stress ratio *R* on the threshold could be ignored, and the fatigue threshold for $R \geq 0.5$ could be applied (Hobbacher 2015). The mean value of K_{th} is obtained from the tests performed by Austen (1983), while the standard deviation is calculated by the coefficient of variation determined after Walbridge (2005).

In the case of the initial flaws, since the semi-elliptical model is employed, the depth and width of initial flaws (a_0 and c_0) are considered. In order to reflect the correlation between the two sizes, the initial flaw size is described by the size parameter a_0 and the ratio parameter a_0/c_0. The distributions of the two parameters are obtained from the study by Kountouris (1989). The space between initiation sites C_{sp} is assumed to be a deterministic value of 1 mm (Madia et al. 2018). Thus, the number of initiation sites C_{num} could be determined by the length of joint W and the space C_{sp}. Table 4 summarizes the distributions of the variables in the probabilistic model.

Table 3 Distribution of local geometries

Code	θ (°)	L (mm)	$\bar{\theta}$	S_θ	$\bar{L}$	S_L
CU1	65	8.01	61	5.3	9.8	2.5
CU2	62	10.65				
CU3	65	6.46				
CU4	52	12.54				
CU5	61	11.53				
TEU1	63	10.58	53	7.5	13.1	2.1
TEU2	54	12.29				
TEU3	45	15.85				
TEU4	53	12.52				
TEU5	44	15.53				
TEU6	59	11.90				

Table 4 Summary of variables in the probabilistic model

Type	Variable	Symbol	Unit	Distribution	μ	σ
Material Properties	stage 1 growth rate	A_1	N/mm$^{3/2}$	Lognormal	6.30×10^{-18}	5.36×10^{-18}
	stage 1 power	m_1	/1*	Deterministic	5.10	0
	stage 2 growth rate	A_2	N/mm$^{3/2}$	Lognormal	6.33×10^{-13}	2.60×10^{-13}
	stage 2 power	m_2	/1	Deterministic	2.88	0
	Threshold	ΔK_{th}	N/mm$^{3/2}$	Lognormal	140	21
	Transition threshold	ΔK_{tr}	N/mm$^{3/2}$	Dependent		
Welded joint geometries	Thickness	T	/mm	Deterministic	16	0
	Joint length	W	/mm	Deterministic	600	0
	Leg length-CU	L	/mm	Normal	9.8	2.5
	Leg length-TEU			Normal	13.1	2.1
	Weld angle-CU	θ	/degree	Normal	61	5.3
	Weld angle-TEU			Normal	53	7.5
Initial flaw	Crack depth	a_0	/mm	Lognormal	0.15	0.10
	Crack ratio	a_0/c_0	/1	Lognormal	0.62	0.25
	Crack space	C_{sp}	/mm	Deterministic	1	0
	Crack number	C_{num}	/1	Dependent		

*/1: Unitless

3.3 Computational procedures

By combining the proposed crack growth model with the probabilistic model, a probabilistic assessment model is established. The model is coded in MATLAB software (MATLAB 2018), and the computational procedures are illustrated in Fig. 11. At the first stage, sampling of parameters is carried out using the established probabilistic model, including the material properties, initial flaws and local geometries. Meanwhile, the finite element (FE) model is established using the local geometries generated by the sampling, to calculate the stress in the joint. The sampled parameters, along with the stress results calculated by the FE model, are then input to the crack growth model.

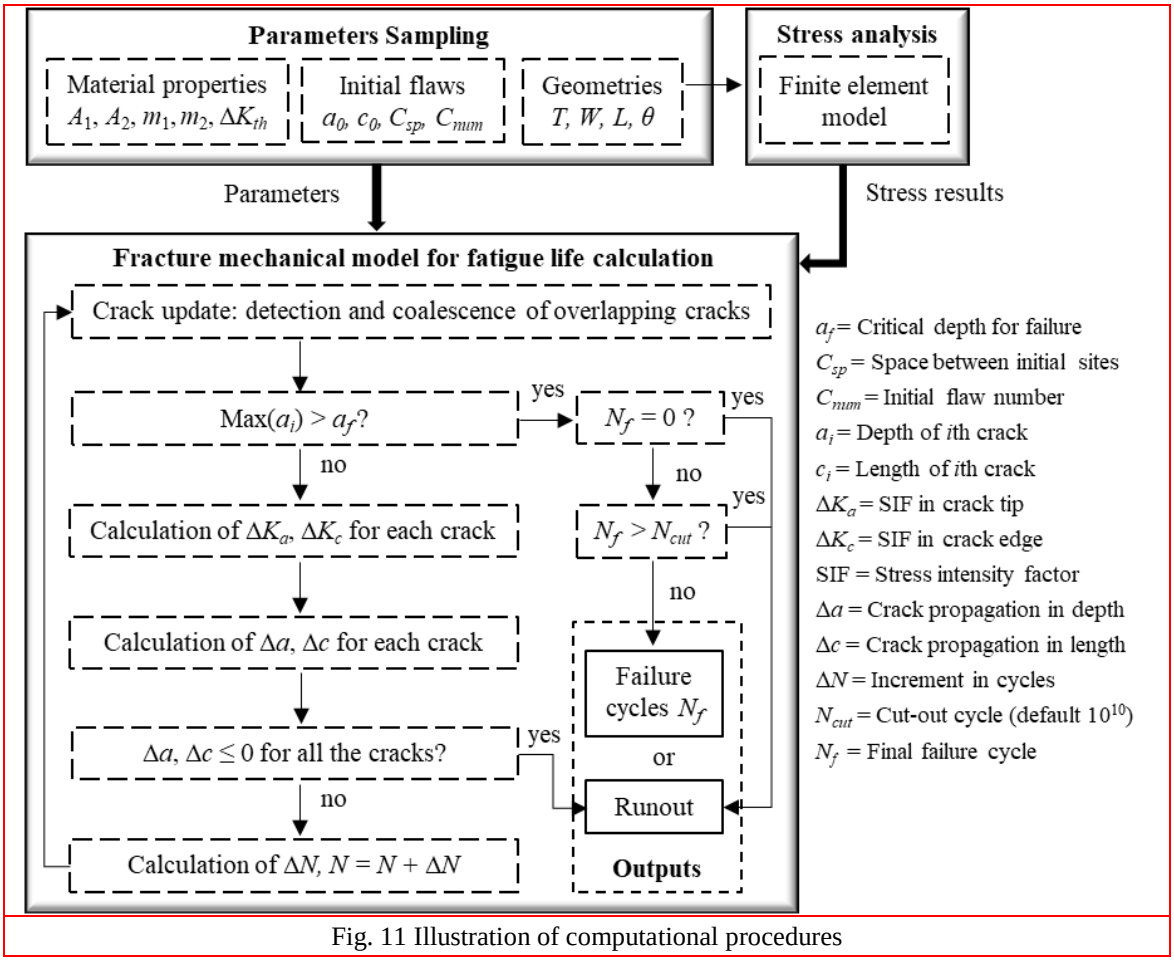

Fig. 11 Illustration of computational procedures

The calculation of crack growth is running step-by-step. At the beginning of each step, the overlapping cracks are detected and then merged using the criterion stated before. In the following, the stress intensity factors are solved for each crack, and then subsequently used to calculate the increments in cracking depth and width. If the increments in both directions are zero for all the cracks, indicating the cracks will not develop, the simulation is then stopped and taken as a run-out. Otherwise, the increment in cycles will be calculated, and the fatigue life will be updated. It is worth noting that, for the accuracy purpose, the increment in cycles is adjusted by the maximum

limits on the increment in crack sizes, which are 0.001 mm for the depth and 0.01 mm for the width in this study. The calculation continues until the critical depth is achieved. In accordance with the failure criterion used in the fatigue test, the critical depth is set as the thickness of the deck plate, i.e., 16 mm. In another word, failure is assumed to be achieved when the crack penetrates through the thickness of deck plates. According to Liu and Mahadevan (2009), a cut-out limit of 10^{10} is set in calculating the fatigue life, over which the simulation is considered as a run-out. In the most extreme case, the maximum depth of initial flaws may exceed the critical depth, which could be regarded as the small possibility event. Under this situation, the fatigue life is assumed to be zero, and the simulation is also taken as a run-out.

4. Validation of the probabilistic assessment model

4.1 Development and verification of the finite element model

Finite element (FE) models are established using the ANSYS software (ANSYS 2018a) to calculate the stress results, as shown in Fig. 12. The testing platform is modelled using the 3D shell element SHELL181. The specimen, rubber plate and cover plate are modelled using the 20 nodes solid element SOLID186. Refined meshing is employed for the rib-to-deck joint of interest, using an element size of 1 mm. The high-strength bolts are simulated by the 3D beam element BEAM188. Through the MPC coupling method (ANSYS 2018b), the bolts are tied to the testing platform, specimen and cover plate. Surface-to-surface contact (ANSYS 2018b) is used to simulate the contacting pair between the specimen and testing platform. The rubber plate is tied to the deck plate, and the applied load is simulated by the uniform pressure imposed on its top surface. The fixed boundary is applied on the bottom surface of the testing platform.

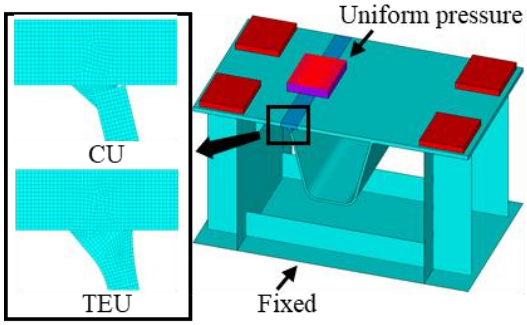

Fig. 12 FE model of specimens

The membrane and bending stress required in Eq. 4 are solved by separating the stress components from the stress results, as shown in Eqs. 10(a) and (b).

$$\sigma_m = \frac{1}{T}\int_0^T \sigma(x)\,dx \ \#(10a)$$

$$\sigma_b = \frac{6}{T^2}\int_0^T (\sigma(x) - \sigma_m)\cdot\left(\frac{T}{2} - x\right)dx \ \#(10b)$$

where σ_m and σ_b are membrane and bending stress respectively; $\sigma(x)$ is the transverse

stress along the thickness of deck plate; T is the thickness of deck plate.

Comparisons of the stress are conducted between the test data and the results obtained by the FE model. Fig. 13 shows the comparison between the specimens CU-5 and TEU-6 at the points D8-X. According to the comparison, the stress data obtained from the FE model match well with the test data at most of the points, indicating that the FE model could be used to calculate the stress in rib-to-deck joints.

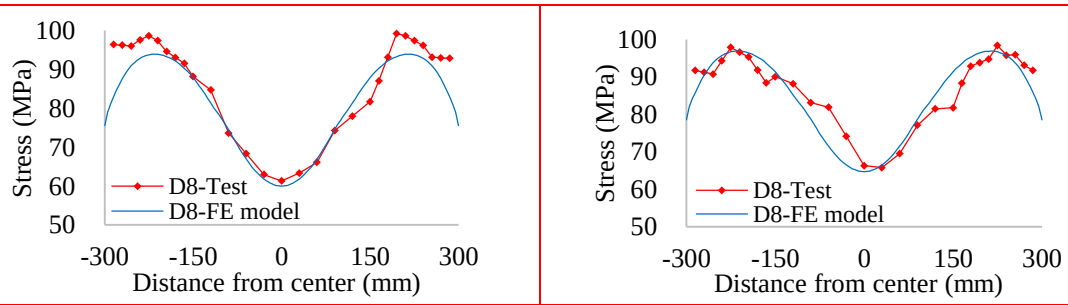

(a) CU-5 (b) TEU-6

Fig. 13 Comparison in stress results

4.2 Comparison in crack propagation and fatigue life

In order to verify the effectiveness of the proposed model in predicting the fatigue life, Monte Carlo (MC) simulations are performed for the specimens using the local geometries measured. According to the principle of large sample size, 500 MC simulations have been conducted for each specimen (Devore 2011). Fig. 14 shows the pattern of crack development, which is obtained using the local geometries of the specimen CU-4. It shows that two main cracks are formed from the initial flaws existed along the joint. The crack emerging earlier first penetrates through thickness and reaches the critical depth. Compared with the cracking pattern measured from tests, it shows that the cracking location could be correctly predicted without a pre-setting cracking site when using the proposed model. Meanwhile, the cracking pattern obtained by the model is in high accordance with that measured in the tests.

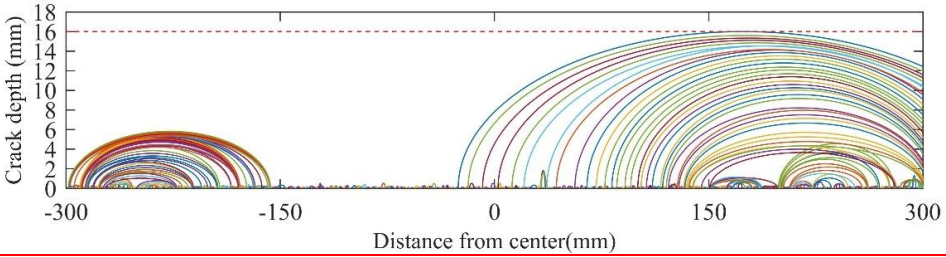

Fig. 14 Pattern of crack development obtained by the proposed model (CU-4)

For further verification, comparisons have also been performed between the prediction and test in terms of the failure cycles and equivalent fatigue strength. The prediction results are fitted by specific distributions. It is found that the lognormal distribution is suitable for the distribution of failure cycles, while the normal distribution is suitable for the distribution of equivalent fatigue

strength. Similar conclusions could be found in the literature about the statistics on fatigue tests (Shen 1994). Figs. 15 and 16(a)-(b) shows the distributions of the specimen TEU-6.

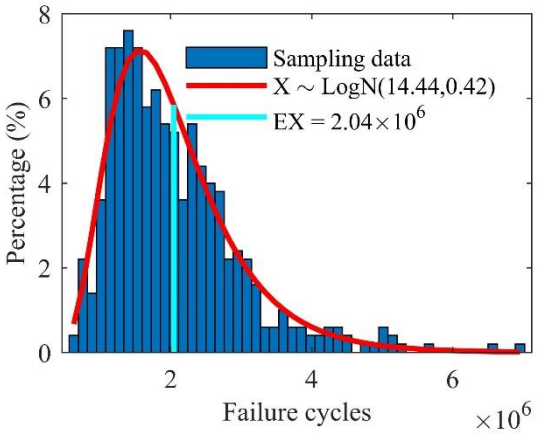

Fig. 15 Distribution of failure cycles (TEU-6)

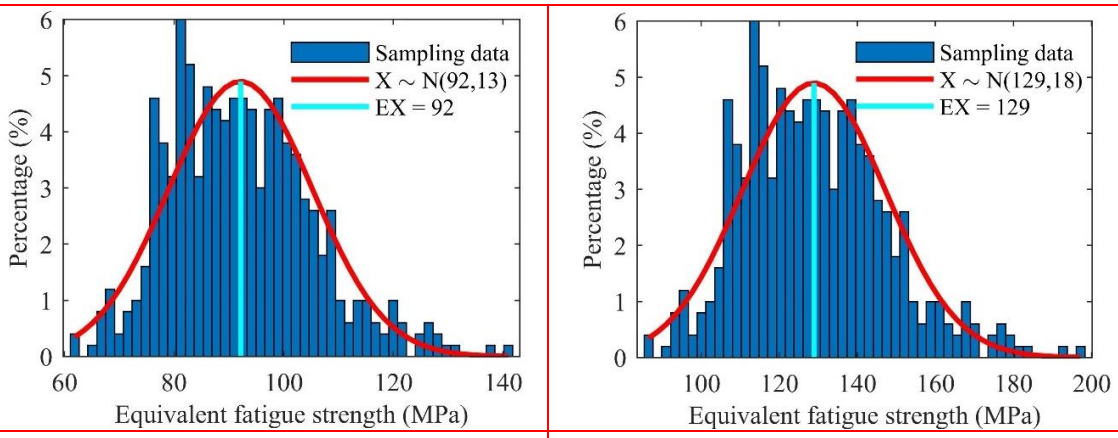

(a) Nominal stress (b) Hot spot stress

Fig. 16 Distribution of equivalent fatigue strength (TEU-6)

Unlike the deterministic analysis, the prediction results are illustrated in distributions rather than deterministic values. Thus, the stochastic nature of fatigue strength could be explicitly considered in the proposed model. In comparison, the prediction interval of the distributions has been employed (Devore 2011), as shown in Eq. 11.

$$PI_\alpha = \bar{x} \pm t_{\alpha/2,n-1} \cdot s\sqrt{1+1/n} \#(11)$$

where PI_α is the prediction interval under $100(1-\alpha)\%$ prediction level; $\bar{x}$ stands for the sample mean; $t_{\alpha/2,n-1}$ is the two-sided critical value of t-distribution with $n-1$ degrees at level α; s stands for the sample standard deviation; n is the sample size.

As a common practice, the possibility of 5% is regarded as the threshold of small probability events, which are unlikely to happen in a single trial (Devore 2011). Correspondingly, the test data

are likely to fall into the 95% PI in a single trial if the model could simulate the test. Thus, the 95% PI could be employed to verify the effectiveness of the prediction model. On this ground, the 95% PI has been employed. The results are plotted against the test data in Figs. 17 and 18(a)-(b).

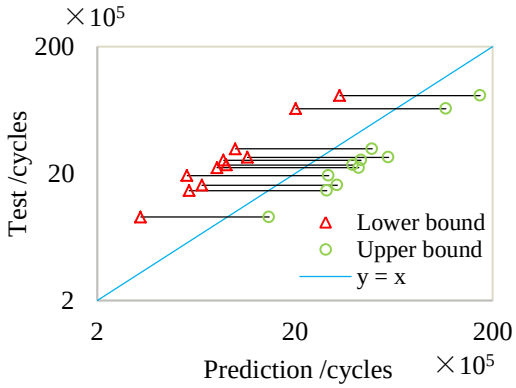

Fig. 17 Comparison in failure cycles

The lower and upper bound of the PIs are represented by red triangles and green circles respectively, while the blue line stands for the situation that the predicted and testing value are completely the same. As the result, all the connecting lines between lower and upper bounds intersect the blue line, indicating that all the test data are within the prediction intervals. Meanwhile, the upper bounds are closer to the blue line than the lower bounds, demonstrating that the results obtained by the model are relatively conservative compared with the test data.

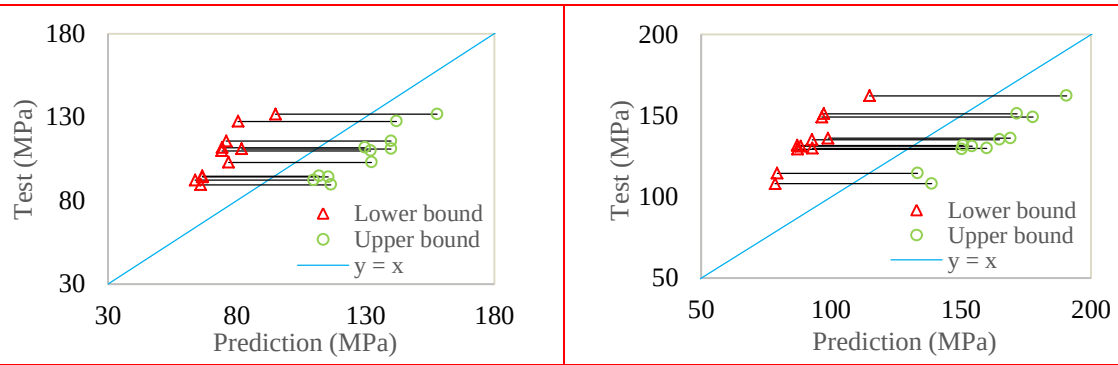

(a) Nominal stress (b) Hot spot stress

Fig. 18 Comparison in equivalent failure strength

5. Derivation of numerical stress-life curves

5.1 Generation of larger-scale fatigue data

Through the proposed assessment model, numerical stress-life design curves have been derived under the specified survival rate. The derivation procedures are shown in Fig. 19. At first, a set of

stress levels are selected and the number of Monte Carlo (MC) simulations on each stress level are determined. After that, stress-life data are generated at the chosen stress levels by the MC runs using the proposed model.

In the full-scale fatigue test, even if the test is running 24 hours a day and 7 days a week, it may take almost one or more weeks to test a single specimen. At the same time, the manufacturing and labour costs of the fatigue test are extensive, which further restrict its application. Alternatively, using the proposed model, a stress-life data point could be generated within only five seconds when a 4-cores desktop (i7-7700K) is used. Thus, it becomes much feasible to obtain a large-scale fatigue database. Regression analysis is then performed on the obtained database to derive the numerical curves using the method stated in section 2.3. It is worth noting that the power index m is no longer assumed but calculated by the least square method since the large-scale database is available.

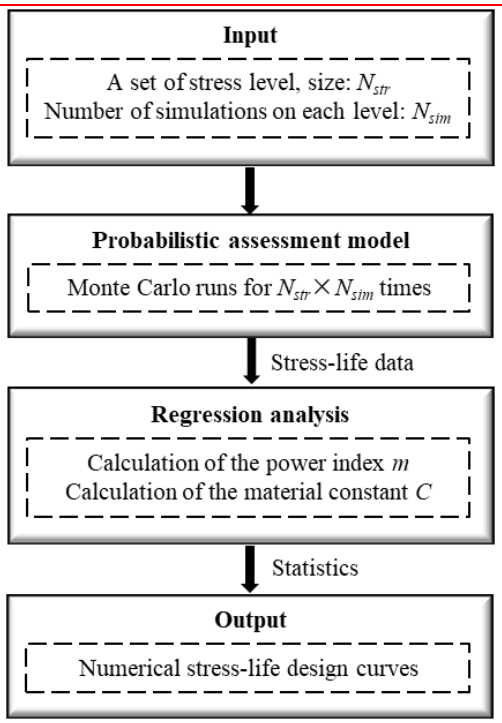

Fig. 19 Derivation of numerical stress-life curves

5.2 Results and discussion

Numerical stress-life curves have been derived for both the CU and TEU specimens, in terms of nominal and hot spot stress. As shown in Figs. 20 and 21, the obtained data are plotted against the mean curves and design curves. The fatigue strength at 2 million cycles (FAT) is also calculated basing on the curves and included in Figs. 20 and 21. In the case of nominal stress, the power indexes of 2.92 and 2.89 have been obtained for the CU and TEU specimens respectively, which are close to the value of 3.0 assumed in the tests. Meanwhile, in case of nominal stress, the

mean FAT of TEU specimens is 22% higher than that of CU specimens, while their design FAT is 23% higher than that of CU specimens. As it turns to hot spot stress, the power indexes are the same, while the TEU specimens have the mean FAT 18% higher and the design FAT 22% higher compared with the CU specimens.

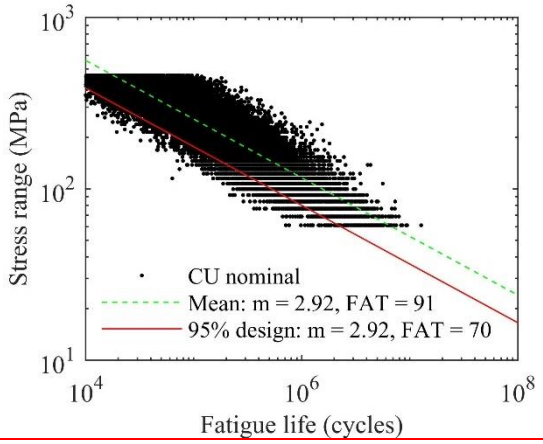

(a) CU specimens

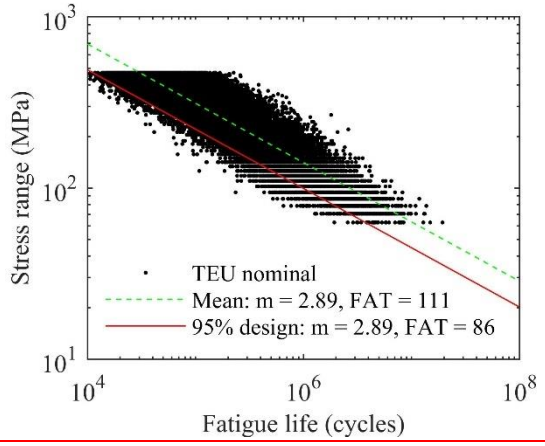

(b) TEU specimens

Fig. 20 Nominal stress-life curves

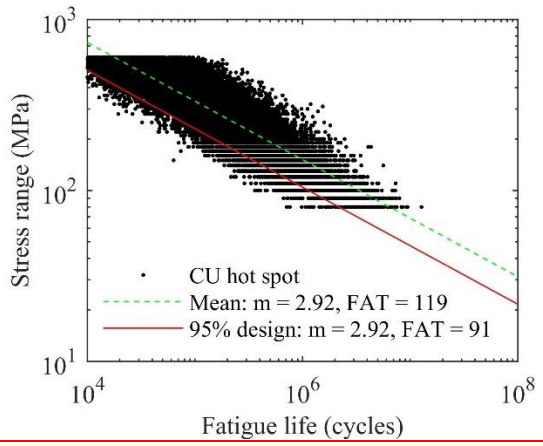

(a) CU specimens

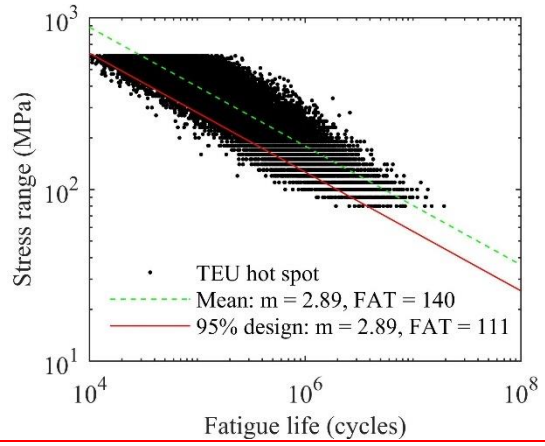

(b) TEU specimens

Fig. 21 Hot spot stress-life curves

The comparison could also be conducted between the numerical data and the test result shown in Figs 7(a) and (b). In the case of mean curves, the numerical results match well with the test data in terms of both the FAT and power index. The maximum difference in the FATs is no more than 5%. However, in terms of the design curve, the numerical result has the FATs relatively lower than those of the test result, indicating the higher randomness is achieved in the numerical data. Given that the sample size of the fatigue test is limited, the test data are not enough to account for the randomness in the fatigue strength. As a result, a small deviation may be generated when using the test data only. In contrast, a higher scatter has been obtained with the large-scale data generated by

the proposed model, indicating that the numerical result is relatively conservative. The same conclusion has also been illustrated in section 4.2.

Thus, it is safe to apply the numerical design curves in the fatigue design of rib-to-deck joints. After rounding, the FAT 85 and FAT 110 curves with the power index *m* of 2.89 are recommended in fatigue evaluation on rib-to-deck joints using TEUs in terms of nominal stress and hot spot stress respectively. At the same time, the FAT 70 and FAT 90 curves with $m = 2.92$ are suggested for the evaluation on rib-to-deck joints using CUs in terms of nominal stress and hot spot stress respectively.

5. Conclusions

Based on the above studies, the conclusions can be drawn as follows:

- Full-scale fatigue tests have been carried out for rib-to-deck joints using thickened edge U-ribs (TEUs) and those using conventional U-ribs (CUs). According to the test, the mean fatigue strength of TEU specimens is 21% and 17% higher than that of CU specimens in terms of nominal and hot spot stress, respectively. In the case of design curves, the FAT values of TEU specimens are 19% higher than that of CU specimens in terms of both nominal and hot spot stress.
- The propagation of fatigue cracks has been measured using the strain gauges installed along the joint. The result shows that two major cracks will initiate and propagate near both ends of the specimen, while the one occurs first will penetrate the deck plate cause the fatigue failure eventually. Meanwhile, the crack almost remains in the semi-elliptical shape during the development.
- Instead of the traditional deterministic analysis, a probabilistic assessment model has been established on the basis of the test data, to predict the fatigue life of rib-to-deck joints. In the model, the randomness in the material properties, initial flaws and local geometries are considered, through which the stochastic nature of fatigue could be better accounted for. Meanwhile, multiple-sites initiation and coalescence of cracks are also considered in the crack growth model, for which the pre-definition of the cracking site is avoided.
- Comparisons have been performed between the test data and predictions made by the proposed model. The result shows that the cracking pattern obtained by the model are in high accordance with that measured in the test. Meanwhile, through the comparisons in fatigue life and equivalent fatigue strength, the proposed model demonstrates the satisfied accuracy in prediction.
- Through employing the proposed model, large-scale databases of fatigue life could be generated in a short period, and then used to derive the mean curve and design curve. Comparisons are made between the test data and numerical results. The result highlights that the two data are in a good match in terms of mean curves, while the numerical results are relatively conservative in terms of design curves. Thus, the numerical design curves could be safely used as references in the fatigue design of rib-to-deck joints.
- Based on this study, the FAT 85 and FAT 110 curves with the power index *m* of 2.89 are recommended in the fatigue evaluation on the rib-to-deck joint using TEUs in terms of nominal stress and hot spot stress respectively. Meanwhile, the FAT 70 and FAT 90 curves with $m = 2.92$ are suggested in evaluation on the rib-to-deck joint using CUs in terms of nominal stress and hot spot stress respectively.

Acknowledgments

The study is supported by the National Natural Science Foundation of China (grant number: 51778536, Doctoral Innovation Fund Program of Southwest Jiaotong University (grant number: D-CX201701), the Zhejiang Department of Transportation (grant number: 10115066), China Scholarship Council and British Council through the Newton Fund. The first author would like to express his sincere thanks to Prof. Yongming Liu at Arizona State University, for his kind help on the probabilistic fatigue assessment model.

References

Anderson, T.L. (2005), *Fracture Mechanics: Fundamentals and Applications (Third Edition)*, CRC press, Baca Raton, FL, USA.

ANSYS (2018a), Engineering Simulation and 3D Design Software; ANSYS Inc., Canonsburg, USA. http://www.ansys.com/

ANSYS (2018b), *Mechanical APDL Documentation*, ANSYS Inc., Canonsburg, PA, USA.

Austen, I. (1983), "Measurement of fatigue crack threshold value for use in design", BSC Report SH/EN/9708/2/83/B; British Steel Corporation, London, UK.

Baptista, C., Reis, A. and Nussbaumer, A. (2017), "Probabilistic S-N curves for constant and variable amplitude", *Int. J. Fatigue*, **101**, 312-327. https://doi.org/10.1016/j.ijfatigue.2017.01.022.

Baik, B., Yamada, K. and Ishikawa, T. (2011), "Fatigue crack propagation analysis for welded joint subjected to bending", *Int. J. Fatigue*, **33**(5), 746-758. https://doi.org/10.1016/j.ijfatigue.2010.12.002.

Bing, W., Pengmin, L. and Yuhong, S. (2015), "Research on rib-to-diaphragm welded connection by means of hot spot stress approach", *Steel Comp. Struct.*, **18**(1), 135-148. https://doi.org/10.12989/scs.2015.18.1.135.

Bing, W., Qiao, H. amd Xiaoling, L. (2017), "Deterioration in strength of studs based on two-parameter fatigue failure criterion", *Steel Comp. Struct.*, **23**(2), 239-250. https://doi.org/10.12989/scs.2017.23.2.239.

Bowness, D. and Lee, M.M.K. (2000). "Prediction of weld toe magnification factors for semi-elliptical cracks in T–butt joints", *Int. J. Fatigue*, **22**(5), 369-387. https://doi.org/10.1016/S0142-1123(00)00012-8.

BS 7910 (2015), Guide to methods for assessing the acceptability of flaws in metallic structures, British Standards Institution; BSI Standards Limited, London, UK.

Cao, V.D., Sasaki, E., Tajima, K. and Suzuki, T. (2015), "Investigations on the effect of weld penetration on fatigue strength of rib-to-deck welded joints in orthotropic steel decks." *Int. J. Steel Struct.*, **15**(2), 299-310. https://doi.org/10.1007/s13296-014-1103-4.

Chen, X., Qingtian S. and Hiroshi, M. (2017), "Static and fatigue performance of stud shear connector in steel fiber reinforced concrete", *Steel Comp. Struct.*, **24**(4), 467-479. https://doi.org/10.12989/scs.2017.24.4.467.

Connor, R., Fisher, J., Gatti, W., Gopalaratnam, V., Kozy, B., Leshko, B., McQuaid, D.L., Medlock, R., Mertz, D., Murphy, T., Paterson, D., Sorensen, O. and Yadlosky, J. (2012), "Manual for design, construction, and maintenance of orthotropic steel deck bridges", FHWA Report FHWA-IF-12-027; HDR Engineering Inc., Pittsburgh, USA.

Devore, J. (2011), *Probability and Statistics for Engineering and the Sciences (Ninth Edition)*, Cengage learning, Boston, MA, USA.

Eurocode (2005), Design of steel structures, Part 1-9: Fatigue, European Committee for Standardization; Brussels, Belgium.

GB/T 714 (2015), Structural steel for bridge, Standardization Administration of the People's Republic of China, Beijing, China.

Heng, J., Zheng, K., Gou, C., Zhang, Y. and Bao, Y. (2017), "Fatigue performance of rib-to-deck joints in orthotropic steel decks with thickened edge U-ribs", *J. Bridge Eng.*, **22**(9), 04017059.

https://doi.org/10.1061/(ASCE)BE.1943-5592.0001095.
Heng, J., Zheng, K., Zhang, Y., Wang, Y. (2018), "Enhancing fatigue performance of rib-to-deck joints in orthotropic steel decks using thickened edge u-ribs", *Proceedings of Structures Congress 2018*, Fort Worth, USA, April. https://doi.org/10.1061/9780784481332.032.
Hobbacher, A. (2015), *Recommendations for Fatigue Design of Welded Joints and Components*, Springer, Basel, Switzerland. https://doi.org/10.1007/978-3-319-23757-2.
JGJ 82-2011 (2011), Technical specification for high strength bolt connections of steel structures, Ministry of Housing and Urban-Rural Development of the People's Republic of China, Beijing, China.
Kainuma, S., Yang, M., Jeong, Y. S., Inokuchi, S., Kawabata, A. and Uchida, D. (2016), "Experiment on fatigue behavior of rib-to-deck weld root in orthotropic steel decks", *J. Constr. Steel Res.*, **119**, 113-122. https://doi.org/10.1016/j.jcsr.2015.11.014.
Kamaya, M. (2008), "Growth evaluation of multiple interacting surface cracks. Part I: Experiments and simulation of coalesced crack", *Eng. Fract. Mech.*, **75**(6), 1336-1349. https://doi.org/10.1016/j.engfracmech.2007.07.015
Kountouris, I.S. and Baker, M.J. (1989), "Defect assessment: analysis of the dimensions of defects detected by ultrasonic inspection in an offshore structure", CESLIC Report OR8; Imperial College of Science and Technology, London, UK.
Liu, Y. and Mahadevan, S. (2009), "Probabilistic fatigue life prediction using an equivalent initial flaw size distribution", *Int. J. Fatigue*, **31**(3), 476-487. https://doi.org/10.1016/j.ijfatigue.2008.06.005.
Luo, P., Zhang, Q., Gong, D., Bu, Y. and Ye, Z. (2018), "Study of fatigue performance of u rib-to-deck double-side welded joint in orthotropic steel bridge deck", *Bridge Constr.*, **2018**(2), 19-24. (In Chinese)
Madia, M., Zerbst, U., Beier, H. T. and Schork, B. (2018), "The IBESS model–Elements, realisation and validation", *Eng. Fract. Mech.*, **198**, 171-208. https://doi.org/10.1016/j.engfracmech.2017.08.033.
Maljaars, J. and Vrouwenvelder, A. C. W. M. (2014), "Probabilistic fatigue life updating accounting for inspections of multiple critical locations", *Int. J. Fatigue*, **68**, 24-37. https://doi.org/10.1016/j.ijfatigue.2014.06.011.
MATLAB (2018), Programming language; MathWorks, Natick, MA, USA. https://www.mathworks.com/
Meng, W., Valipour, M. and Khayat, K.H. (2016), "Optimization and performance of cost-effective ultra-high performance concrete", *Mater. Struct.*, **50**(1), 29. https://doi.org/10.1617/s11527-016-0896-3.
Mukherjee, S. and Roy, S. (2015), "Fatigue evaluation of a steel orthotropic deck for a lift bridge by laboratory testing of a full scale prototype", *Proceedings of Structures Congress 2015*, Portland, USA, April.
Nagy, W., Van Bogaert, P. and De Backer, H. (2015), "LEFM based fatigue design for welded connections in orthotropic steel bridge decks", *Fatigue Design 2015*, Senlis, France, November.
Niemi E., Fricke W. and Maddox S. J. (2006), *Structural Hot-Spot Stress Approach to Fatigue Analysis of Welded Components*, Woodhead Publishing, Cambridge, UK.
Pang, J.H., Hoh, H.J., Tsang, K.S., Low, J., Kong, S.C., and Yuan, W.G. (2017), "Fatigue crack propagation analysis for multiple weld toe cracks in cut-out fatigue test specimens from a girth welded pipe", *Int. J. Fatigue*, **94**, 158-165. https://doi.org/10.1016/j.ijfatigue.2016.09.011.
Qinghua, H., Yihong, W., Jie, X. and Ying, X. (2016), "Fatigue behavior of stud shear connectors in steel and recycled tyre rubber-filled concrete composite beams", *Steel Comp. Struct.*, **22**(2), 353-368. https://doi.org/10.12989/scs.2016.22.2.353.
Righiniotis, T.D. and Chryssanthopoulos, M.K. (2003), "Probabilistic fatigue analysis under constant amplitude loading", *J. Constr. Steel Res.*, **59**(7), 867-886. https://doi.org/10.1016/S0143-974X(03)00002-6.
Sanches, R.F., de Jesus, A.M., Correia, J.A., Da Silva, A.L.L. and Fernandes, A.A. (2015), "A probabilistic fatigue approach for riveted joints using Monte Carlo simulation", *J. Constr. Steel Res.*, **110**, 149-162. https://doi.org/10.1016/j.jcsr.2015.02.019.
Shen, C. (1994), "The statistical analysis of fatigue data", Ph.D. Dissertation, The University of Arizona, Tucson, USA.
Tang, M.C. (2011), "A new concept of orthotropic steel bridge deck", *Struct. Infrastruct. E.*, **7**(7-8), 587-595.

https://doi.org/10.1080/15732479.2010.496996.
Walbridge, S. (2005), "A probabilistic study of fatigue in post-weld treated tubular bridge structures", Ph.D. Dissertation, EPFL, Lausanne, Switzerland.
Xiaochen, J. and Zhibing Z. (2014), "Study on uplift performance of stud connector in steel-concrete composite structures", *Steel Comp. Struct.*, **18**(5), 1279-1290. https://doi.org/10.12989/scs.2015.18.5.1279.
Zhang, Q., Liu, Y., Bao, Y., Jia, D., Bu, Y. and Li, Q. (2017), "Fatigue performance of orthotropic steel-concrete composite deck with large-size longitudinal U-shaped ribs", *Eng. Struct.*, **150**, 864-874. https://doi.org/10.1016/j.engstruct.2017.07.094.